ISSN 2616-5767 Vol.7, Issue 6: 111-116, DOI: 10.25236/AJETS.2024.070616

Numerical Simulation of Residual Stress and Deformation in Electron Beam Welded Joints of 40CrNiMoA Alloy

Jiahao Zhang, Minghai Li

School of Zhan Tianyou, Dalian Jiaotong University, Dalian, 116028, China
jiahao513.zhang@outlook.com

Abstract: *To investigate the residual stress and deformation behavior of 40CrNiMoA alloy joints during the process of cylindrical docking electron beam welding. A combined heat source model of planar Gaussian and Gaussian rotating body was used to simulate the electron beam welding process of a 6mm thick 40CrNiMoA alloy rectangular plate. The residual stress and deformation distribution of the welded joint under two process parameters, low beam low welding speed and high beam high welding speed, were compared and studied. Under high beam current and high welding speed parameters, a weld seam with high aspect ratio, small high stress concentration area, and small deformation was obtained; Under this parameter, the size of the high stress concentration area on the cross-section of the weld seam is relatively small, with a width of only 84% of that under low beam and low welding speed parameters; Meanwhile, under high beam current and high welding speed parameters, the maximum deformation of the weld seam is 0.2387mm, which is lower than the 0.2655mm under low beam current and low welding speed parameters. The high beam high welding speed process has the characteristics of heat concentration, low heat input, and high processing efficiency, which is more conducive to obtaining welds with small stress concentration areas, small deformation, and high aspect ratios. It has more processing advantages than the low beam low welding speed process.*

Keywords: *40CrNiMoA alloy; welding deformation； numerical simulation; electron beam welding; residual stress*

1. Introduction

Because 40CrNiMoA steel has good strength and toughness, as well as excellent hardenability and thermal stability, it is now suitable for manufacturing important parts with high strength requirements and mainly used in fields such as weapons and equipment, automobiles, aerospace, etc. However, as a critical component of various types of equipment, the application environment of 40CrNiMoA alloy steel is increasingly valued and often requires welding before use. The microstructure of various parts of the 40CrNiMoA weld seam varies greatly, which can easily generate large residual stresses. In practical engineering, adjusting the post weld heat treatment can improve the microstructure of the weld seam, eliminate residual stress, thereby improving the plasticity and fracture toughness of the joint, and enhancing its stress corrosion resistance[1].

40CrNiMoA alloy is a new generation of high-strength alloy material, which has comprehensive mechanical properties such as high strength, excellent wear resistance, and ductility. It also has good hardenability and mechanical processing performance, and is widely used in automotive parts, heavy machinery parts, and tools[2]. At present, the commonly used welding methods for 40CrNiMoA alloy are laser welding, electron beam welding, friction welding, diffusion welding, and other welding processes with extremely high energy density. Among various welding processes, electron beam welding has the advantages of strong electron beam penetration ability, high energy density, small welding deformation, and high welding efficiency[3-5], making it the preferred welding process for 40CrNiMoA alloy welding.

To solve the stress concentration problem in the electron beam welding process of 40CrNiMoA alloy and avoid the problem of weld cracking caused by the synergistic effect of stress and brittle intermetallic compounds, it is necessary to study the influence of residual stress and deformation after welding. Conventional testing methods have significant limitations in studying residual stress and deformation of welds, and the detection cost is expensive, making it difficult to study the stress field of the entire weld. After conducting initial heat source verification and other experiments on 40CrNiMoA alloy using finite

ISSN 2616-5767 Vol.7, Issue 6: 111-116, DOI: 10.25236/AJETS.2024.070616

element method, finite element simulation was carried out to simulate the stress field and deformation field of the weld seam, in order to study the distribution law of residual stress field and deformation field after welding[6-8].

This project takes 6 mm thick 40CrNiMoA alloy as the research object, uses numerical simulation method to compare and analyze the residual stress and deformation during the welding process, and conducts experimental verification, providing theoretical basis for improving the electron beam welding process of 40CrNiMoA alloy, reducing welding costs, and achieving high-quality, crack free welding.

2. Establishment of Finite Element Model

2.1 Establishment of Flat Model and Grid Division

The experimental material selected is 40CrNiMoA alloy, with the following chemical composition:

C: 0.36~0.44, Si: 0.17-0.37, Mn: 0.50-0.80, Cr: 0.6-0.9, Mo: 0.15-0.25, Ni: 1.25-1.75, S≤0.015, P≤0.025, Cu≤0.25.

Establish a three-dimensional finite element model based on the size of the test plate. In response to the non-uniform heating of the test plate during welding, which leads to significant temperature gradient differences in each region, it is necessary to use gradient grids to partition the finite element model. In order to meet the needs of numerical simulation, high-precision calculations need to be performed on the weld area, thus requiring denser mesh partitioning; Due to the fact that the farther away from the weld zone, the smaller the temperature gradient and the slower the energy transfer, a sparser grid mesh is required; Under the condition of meeting the calculation accuracy, the transition zone between the near weld and the weld interval can be appropriately reduced in the number of grids[9] .The size of the experimental model during butt welding is 110mm × 40mm × 6mm. The mesh division of the model is shown in *Figure 1*, and a hexahedral DC3D8 mesh is used to ensure accuracy and computational efficiency during simulation, reducing the possibility of calculation nonconvergence during the simulation process. The number of solid elements in the three-dimensional mesh is 33120.

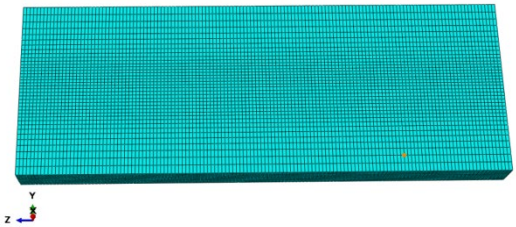

Figure 1 Finite Element Model of Electron Beam Welding Process for 40CrNiMoA Alloy Test Plate

2.2 Establishment of Heat Source Model

Based on the analysis of current research results, it can be concluded that in order to match the high-energy distribution of electron beam welding and the "wide top and narrow bottom" V-shaped melt pool morphology, the combination heat source model of Gaussian surface (see equation (1)) and Gaussian rotating body (see equation (2)) is more suitable for the electron beam welding process of 40CrNiMoA alloy test plates.

$$q_1(x,y) = \frac{3Q_1}{\pi {R_1}^2} e^{\frac{3}{R_1^2}(x^2+y^2)} \tag{1}$$

$$q_2(x,y,z) = \frac{3Q_2}{\pi H {R_2}^2} e^{\frac{3}{R_2^2}(x^2+y^2)} \tag{2}$$

In the formula: q_1 and q_2 are the heat flux densities of Gaussian surface heat source and Gaussian rotating body heat source, respectively; R_1 is the cross-sectional radius of the surface heat source; R_2 is the cross-sectional radius of the body heat source; His the height of the heat source; Q is the laser power, Q =welding voltage×welding current=$Q_1 + Q_2$, where the sizes of Q_1 and Q_2 are determined by the heat input coefficient a, $Q_1 = aQ$, and the heat input distribution coefficient a can be determined by comparing and verifying the actual heat source melt pool with the simulated heat source through a pre

ISSN 2616-5767 Vol.7, Issue 6: 111-116, DOI: 10.25236/AJETS.2024.070616

simulation process. In this paper, $a = 0.2$.

3. Results and Analysis

3.1 Process parameters and boundary conditions

The test panel model is welded with the long side as the surface to be welded. Two sets of process parameters are designed: (1) low beam current and low welding speed with a welding current of 14mA and a welding speed of 8mm/s; (2) A high beam current high welding speed with a welding current of 18mA and a welding speed of 12mm/s. The voltage is 85KV.

Due to the fact that electron beam welding is performed in a vacuum chamber, the boundary conditions for the calculation are set, which means that the test plate (except for the bottom surface) is entirely used for thermal radiation and heat dissipation, and the bottom of the specimen is used as the contact heat transfer area. Welding constraints are set to limit the rigid body rotation and movement at the four corners, and the material parameters of the model are set to be temperature dependent. The mechanical and thermophysical properties of 40CrNiMoA alloy material are shown in the material curve in reference [10], as shown in *Figure 2*.

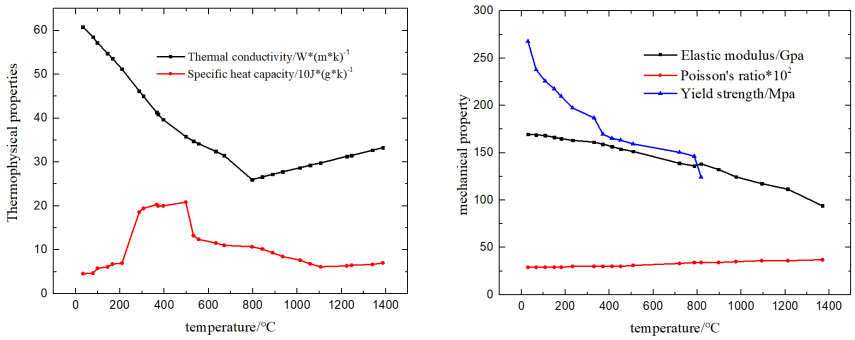

a) Thermal and physical properties *b) mechanical property*

Figure 2 Thermophysical and mechanical properties parameters of 40CrNiMoA alloy

3.2 Welding Temperature Field

The temperature field of the weld surface during the stable welding stage of electron beam welding of 40CrNiMoA alloy is shown in *Figure 3*.It can be seen that under two sets of welding process parameters, the morphology of the welding melt pool at the stable moment of the welding stage is similar to a "teardrop shape". As shown in *Figure 3*a, the peak temperature of the weld pool for the first set of parameters is 3093℃; As shown in *Figure 3b*, the peak temperature of the weld pool for the second set of parameters is 2766℃. The reason is that the welding line energy under the first and second sets of parameters is 1487.5J/cm and 1275J/cm (current× voltage/welding speed), respectively. *Figure 4* shows the thermal cycling curve of the steady-state weld of 40CrNiMoA alloy. The results indicate that under two process conditions, the temperature gradient during the heating stage is very close. However, due to different welding speeds, under high welding speed conditions, the molten pool first heats up and then rapidly decreases; During the cooling process, the cooling gradient of the melt pool is almost the same under the two process parameters.

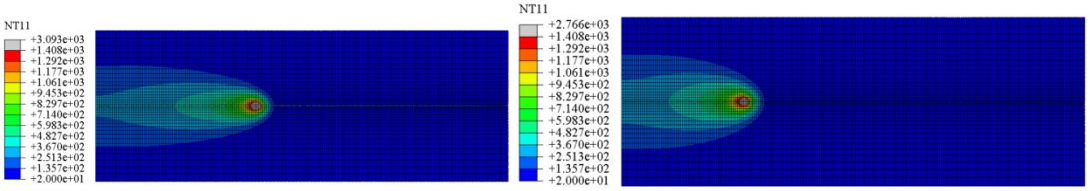

a Low beam current and low welding speed *b High beam current and high welding speed*

Figure 3 Temperature Field on the Surface of Alloy Electron Beam Welding Seam during Stable Welding Stage

ISSN 2616-5767 Vol.7, Issue 6: 111-116, DOI: 10.25236/AJETS.2024.070616

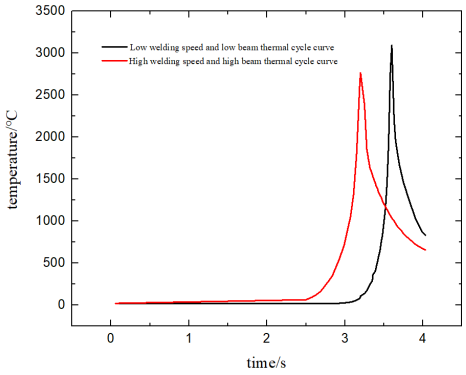

Figure 4 Thermal cycle curve of electron beam stabilized welding section of 40CrNiMoA alloy

As shown in *Figure 5*, the simulated melt pool temperature field under two sets of welding parameters (temperature field cross-section corresponding to time in *Figure 3*), where the area within the fusion line (gray area) is the melt pool area above the simulated calculated temperature of 1408 ℃ (material melting point). The simulation results show that this method can better reflect the microstructure of the welding area. Therefore, the heat source model proposed in this experiment can accurately reflect the morphology and temperature distribution of the molten pool of 40CrNiMoA alloy in electron beam welding. Comparing the shape of the melt pool under two sets of process parameters, as shown in *Figure 5a*, the width of the weld pool under high beam current and high welding speed parameters is 0.77mm, which is smaller than the melt pool width of 0.81mm under low beam current and low welding speed parameters shown in *Figure 5a*. This is because compared with low beam and low welding speed parameters, the welding line energy of the heat source will be smaller when the high beam and high welding speed parameters are used. At the same time, as the welding line energy decreases, the width of the molten pool surface will correspondingly decrease. At the same time, the size of the beam will significantly affect the depth of the molten pool. Increasing the beam size will significantly enhance the penetration ability of the electron beam, thereby increasing the depth of the molten pool; At a higher beam current (18mA), narrow pool width and high aspect ratio welds can be obtained. Therefore, when other welding process parameters are the same, using a high beam high welding speed process can achieve welds with narrower pool width, smaller volume, and higher aspect ratio.

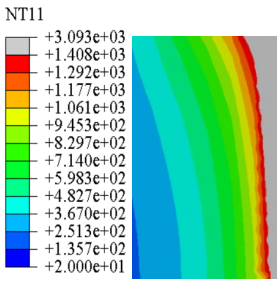

b Low beam current and low welding speed

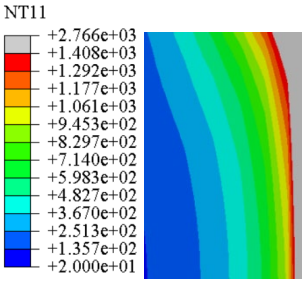

c High beam current and high welding speed

Figure 5 Sectional morphology of electron beam welding seam of 40CrNiMoA alloy

3.3 Residual stress field

Under two sets of parameters, the longitudinal residual stress distribution obtained through simulation is relatively similar (as shown in *Figure 6*), but the high stress concentration areas are different under high beam current and high welding speed parameters and low beam current and low welding speed parameters At positions 2.51mm and 2.98mm respectively, the former is only 84% of the latter. This is because during the welding process, the volume of the molten pool varies. Under low beam and low welding speed parameters, the volume of the molten pool is larger, resulting in a relatively larger distribution range of high stress areas.

The longitudinal residual stress distribution of 40CrNiMoA alloy electron beam weld under high beam current and high welding speed parameters is shown in *Figure 6b*. The residual stress value at the center of the weld is 0MPa, but as it moves away from the weld in the vertical direction, the residual tensile stress value rapidly increases, reaching the highest value of 158.3 MPa at a distance of 2.51mm from the weld. However, at the positions of 2.51-7.5mm, the residual stress value rapidly decreases,

ISSN 2616-5767 Vol.7, Issue 6: 111-116, DOI: 10.25236/AJETS.2024.070616

rapidly transitioning from a high tensile stress state to a compressive stress state of 59.1 MPa; Afterwards, as the distance from the centerline of the weld increases, the longitudinal residual compressive stress gradually decreases to 5 MPa.

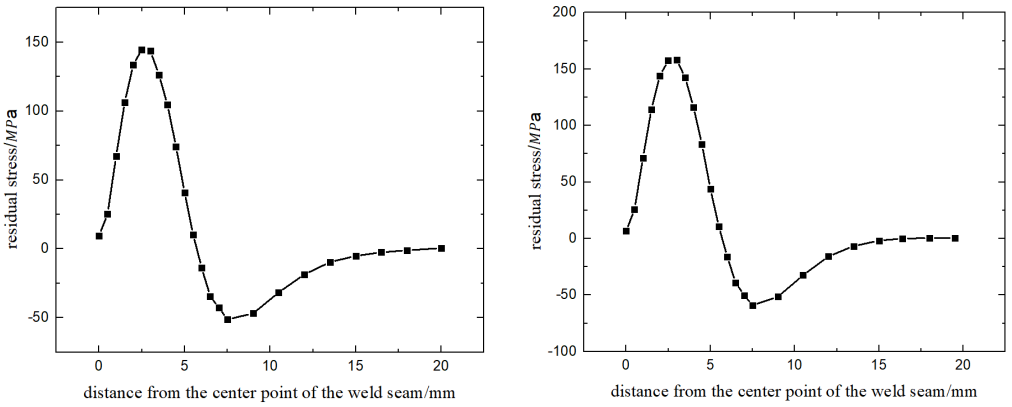

a) Low beam current and low welding speed *b) High beam current and high welding speed*

Figure 6 Longitudinal residual stress distribution curves at different distances from the center of the weld seam

3.4 Post weld deformation field

As shown in *Figure 7*, the cloud maps of the post weld deformation field of 40CrNiMoA alloy under two sets of welding parameters are presented. By observing *Figure 7*, it is found that the distribution pattern of the post weld deformation field under the two sets of parameters is basically the same. Comparing *Figure 7a* and *Figure 7b*, it can be seen that under low beam current and low welding speed parameters, the maximum deformation value is 0.2655 mm, while under high beam current and high welding speed parameters, the maximum deformation value is 0.2387 mm.

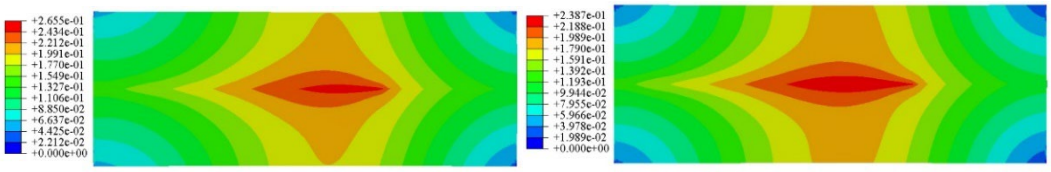

a) Low beam low welding speed deformation field *b) High beam high welding speed deformation field*

Figure 7 Deformation field of electron beam welded joint of 40CrNiMoA alloy

Based on the above, it can be concluded that under high beam current and high welding speed parameters, the welding heat input value is low, the width of the high stress concentration area in the weld seam is narrow, and the volume of the welding pool is small. As a result, the residual deformation of the joint after welding under low beam current and low welding speed parameters is greater than that under high beam current and high welding speed parameters. Based on the above experimental and simulation results, it can be concluded that under high beam current and high welding speed parameters, the initial stage of the temperature cycle curve during the cooling phase has a large amplitude of change, which leads to the generation of significant residual stresses after welding. Therefore, we can observe that the maximum longitudinal residual stress under high beam current and high welding speed parameters is greater than that under low beam current and low welding speed parameters. Under high beam current and high welding speed parameters, the weld pool volume is smaller, the aspect ratio is higher, and the width of the weld pool is narrower, resulting in a smaller transverse heat affected area of the weld. Therefore, under high beam current and high welding speed parameters, the higher stress concentration area of residual stress in the joint is smaller than that under low beam current and low welding speed. At the same time, due to the total heat input of low beam and low welding speed parameters being 1.17 times that of high beam and high welding speed, the heat input is high and there is a large welding pool volume, resulting in a greater residual deformation of the joint after welding under low beam and low welding speed parameters than under high beam and high welding speed. Based on the above analysis, it is found that when the welding speed is appropriate, the parameters of high beam current and high welding speed have the characteristics of relatively concentrated heat, small heat input, and high processing efficiency. They can obtain welds with high aspect ratio, small high stress

ISSN 2616-5767 Vol.7, Issue 6: 111-116, DOI: 10.25236/AJETS.2024.070616

concentration area, and small deformation, which have more process advantages than low beam current and low welding speed parameters.

4. Conclusion

1) This project takes 40CrNiMoA alloy as the research object, and uses a combination of Gaussian rotating body and Gaussian surface heat source method to numerically simulate the electron beam welding process of 40CrNiMoA alloy. The error between the welding residual stress results obtained and the experimental results is within a reasonable range.

2) By comparing the residual stress field results under two sets of process parameters, it was found that under high beam current and high welding speed parameters, the width of the high stress concentration area of the residual stress in the joint was only 84% of that under low beam current and low welding speed parameters.

3) When other welding process parameters are the same, using high beam and high welding speed process parameters can result in narrow melt pool width, small volume melt pool, and high aspect ratio welds.

4) The maximum deformation under low beam current and low welding speed parameters is 0.2655 mm, which is greater than the 0.2387 mm under high beam current and high welding speed parameters. Therefore, the welding deformation under high beam current and high welding speed parameters is relatively small.

References

[1] LIU Zi, KONG Weimin. The influence of post weld local heat treatment area layout on residual stress of thick walled cylindrical circumferential seam[J]. Metal heat treatment,2024,49(09):221-225. DOI:10.13251/j.issn.0254-6051.2024.09.035.

[2] LI Zijian, JIA Limin, HAN Pengbi-ao, et al. The Effect of Heat Treatment Process on the Microstructure and Mechanical Properties of 40CrNiMoA Alloy[J]. Journal of Hebei University of Science and Technology, 2024,45(01):67-73.

[3] LIU Yongqiang, ZHUANG Mingxiang, ZHANG Wenliang, et al. Effect of post weld stress relief on the microstructure and properties of TC4 titanium alloy electron beam welded joints[J]. Electric welding machine, 2023,53(10):22-27.

[4] LI Haidong, XIAO Xuan, LI Haoyuan, et al. Numerical simulation of residual stress and deformation in electron beam welded joints of Ti2AlNb alloy[J]. Precision Forming Engineering,2023,15(08):27-35.

[5] CHEN Shuliang, XU Lei, HU Yuanhao, et al. Research on Numerical Simulation Method of Residual Stress in Aluminum Alloy Pre stretched Plate[J]. computer simulation,2023,40(02):292-296+516.

[6] CHEN Hailong. Research on the microstructure and properties of nickel based coatings prepared by laser cladding on the surface of 40CrNiMoA steel[D]. Liaoning University of Engineering and Technology, 2022. DOI:10.27210/d.cnki.glnju.2022.000068.

[7] CHEN Xiliang. Numerical Simulation of Temperature Field and Deformation in Electron Beam Welding of High Temperature Alloy Ring Parts[D]. Nanchang Hangkong University,2014

[8] LIU Xixia, HUANG Rui, YAO Gang, et al. Numerical simulation of temperature field in laser butt welding of titanium alloy thin plates[J]. Laser technology, 2013,37(05):700-704.

[9] WANG Yongpeng, WANG Shaogang, JIANG Huan, et al, Microstructure and mechanical properties of Al Mg alloy electron beam filled wire welded joints[J]. Material development and application, 2022,37(06):47-54. DOI:10.19515/j.cnki.1003-1545.2022.06.017.

[10] WANG Meiting, ZHENG Li, HE Liang, et al. Numerical simulation of deformation behavior and residual stress of AlSi10Mg alloy formed by SLM[J]. Application of laser, 2022,42(10):67-75. DOI:10.14128/j.cnki.al.20224210.067.